Mechanics of Advanced Composite Structures 2 (2015) 61-72

Mechanics of Advanced Composite Structures

journal homepage: http://macs.journals.semnan.ac.ir

Semnan University

Free Vibration of Lattice Cylindrical Composite Shell Reinforced with Carbon Nano-tubes

J. Emami*, J.E. Jam, M.R. Zamani, A. Davar

Composite Materials and Technology Center, Malek-Ashtar University of Technology, Tehran, Iran

PAPER INFO

Paper history:
Received 31 October 2015
Received in revised form 22 November 2015
Accepted 24 November 2015

Keywords:
Carbon nano-tubes
Lattice structures
Modified Halpin-Tsai equations
Free vibration

ABSTRACT

The free vibration of the lattice cylindrical composite shell reinforced with Carbon Nano-tubes (CNTs) was studied in this study. The theoretical formulations are based on the First-order Shear Deformation Theory (FSDT) and then by enforcing the Galerkin method, natural frequencies are obtained. In order to estimate the material properties of the reinforced polymer with nano-tubes, the modified Halpin-Tsai equations were used and the results were checked with an experimental investigation. Also, the smeared method is employed to superimpose the stiffness contribution of the stiffeners with those of the shell in order to obtain the equivalent stiffness of the whole structure. The effect of the weight fraction of the CNTs and also the ribs angle on the natural frequency of the structure is investigated in two types of length to diameter ratios in the current study. Finally, the results which are obtained from the analytical solution are checked with the FEM method using ABAQUS CAE software, and a good agreement has been seen between the FEM and the analytical results.

1. Introduction

The composite lattice structures have better efficiency and higher strength to weight ratio in comparison with the conventional metal structures. The lattice structures are usually made in the form of the thin-walled cylindrical or conical shells and consist of a system of $\pm\phi$ (with respect to the shell axis) helical and circumferential ribs [1]. The lattice structures are based on the idea of the load carrying skin and buckling. Khalili et al. [2] studied the transient dynamic response of the initially stressed composite circular cylindrical shells under the radial impulse load. They find out that if the axial compressive load increases up to the critical buckling load, the natural frequencies decrease. Hemmatnezhad et al. [3] studied the free vibrations of the grid-stiffened composite cylindrical shells. They worked in both the theoretical and numerical method and used first-order shear deformation theory for analytical solution. Zhang et al. [4] studied the free vibration behaviors of the carbon fiber reinforced lattice-core sandwich cylinder with lattice cores and uni-axial compression, and the free vibration experiments were carried out. The natural frequencies and vibration modes of CFRC LSC were revealed by the experiments for the first time. They find out that the circumferential vibration modes turning from oval, triangle to rectangle lobar mode are dominant in the low primary frequencies, and the beam bending mode appears at higher order.

In the last two decades, many investigations have been conducted into the Carbon Nano-tubes (CNTs). They are known to improve the mechanical stiffness and strength. However, they also should be evaluated in terms of the free vibration of a structure. Zhu et al. [5] carried out the bending and free vibration analyses of the thin-to-moderately thick composite plates reinforced by the single walled carbon nano-tubes. The finite element method was used. Four types of the distributions of

*Corresponding author, Tel.: +98-21-22935300; Fax: +98-21-22936578

E-mail address: javademami90@gmail.com

the uniaxial-aligned reinforcement material are considered. Their results revealed the influences of the volume fractions of the carbon nano-tubes and the edge-to-thickness ratios on the bending responses, natural frequencies and mode shapes of FG-CNTRC plates. Besides, they find the CNTs distributed close to the top and bottom surfaces are more efficient than those distributed near the mid-plane for increasing the stiffness of the plates. Ramgopal Reddy et al. [6] investigated on the free vibration analysis of the carbon nano-tube reinforced laminated composite panels. Three types of panels such as flat, concave and convex are considered and the influence of the boundary conditions on the natural frequency of the CNT reinforced composite panels was analyzed. Aragh et al. [7] worked on the natural frequency analysis of the continuously graded carbon nano-tube-reinforced cylindrical shells based on the third-order shear deformation theory. The interesting finding of their study is that the graded CNT volume fractions with symmetric distribution through the shell thickness have high capabilities to reduce or increase the natural frequency in comparison with the uniformly and asymmetric CNT distribution.

In this study, a new method is introduced for estimating the material property of the composites reinforced with randomly CNTs. Then, the free vibration in both the analytical and FEM analysis is calculated for the lattice cylindrical shell. Eventually, the results of the FEM and analytical method are compared with each other and a good agreement is observed between them.

2. Governing Elastic Properties

When the CNTs are added to the composite, the elastic properties change. Thus, one way to estimate the properties is using modified Halpin-Tsai equations. The Cox model is used to modify these equations. α is the orientation factor in Eqs. (1) and (2) [8]:

$$E_{em}=\frac{1+C\eta V_{CNT}}{1-\eta V_{CNT}}E_m \qquad \eta=\frac{K_w(\alpha E_{CNT}/E_m)-1}{K_w(\alpha E_{CNT}/E_m)+C} \qquad C=2\left(l/d\right) \tag{1}$$

$$G_{em}=\frac{1+C\eta V_{CNT}}{1-\eta V_{CNT}}G_m \qquad \eta=\frac{K_w\alpha\left(G_{CNT}/G_m\right)-1}{K_w\alpha\left(G_{CNT}/G_m\right)+C} \qquad C=\left(l/d\right) \tag{2}$$

where E_m, G_m, K_w, E_{em}, G_{em}, E_{CNT} and G_{CNT} indicate Young's and shear modulus of matrix, the waviness correction factor, Young's and shear modulus of modified polymer, Young's and shear modulus of CNTs respectively.

If the length of reinforcements (CNTs) is greater than the thickness of the specimen, the reinforcements are assumed to be randomly oriented in two dimensions and the factor $\alpha=1/3$ is used. If the length of reinforcements is much smaller than the thickness of the specimen, the reinforcements are assumed to be randomly oriented in three dimensions and the parameter $\alpha=1/6$ is considered [8]. According to the Eqs. (1) and (2), the elastic properties of the polymer which is reinforced with random CNTs can be calculated. Then, substituting the elastic properties of the polymer into the Eqs. (3), (4) and (5), the elastic property of the composite reinforced by CNTs and continuous fibers can be estimated as what follows:

$$E_1=E_rV_r+E_{em}V_{em} \tag{3}$$

$$E_2=\frac{1+C\,\eta V_r}{1-\eta V_r}E_{em}, \quad \eta=\frac{\left(E_r/E_{em}\right)-1}{\left(E_r/E_{em}\right)+C}, \quad C=2\left(l/d\right) \tag{4}$$

$$G_{12}=\frac{1+C\,\eta V_r}{1-\eta V_r}G_{em}, \quad \eta=\frac{\left(G_r/G_{em}\right)-1}{\left(G_r/G_{em}\right)+C}, \quad C=\left(l/d\right) \tag{5}$$

where the constant shape factor C is related to the aspect ratio of reinforcement length l and diameter d. Also, E_r and G_r are the moduli of the reinforcement and V_r is the volume fraction of the reinforcement respectively. In order to validate the above equations, the results are compared with reference [9] which is an experimental investigation and is shown in Table 1.

3. Equivalent Stiffness

In order to calculate the free vibration of the lattice cylindrical composite shell, the equivalent stiffness should be determined. First, a unit cell of the stiffeners which is repeated in the whole of the structure is considered as shown in Fig. 1. Then, with the help of smeared stiffener method and the following refined assumptions, the equivalent stiffness can be calculated [10,11]:

1. The shear stresses in the cross stiffeners are not to be ignored.
2. The cross-section dimensions of the stiffeners are very small compared to the length.
3. A uniform stress distribution is assumed across the cross-sectional area of the stiffeners.
4. The load on the stiffener/shell is transferred through shear forces between the stiffeners and shell.

Table1. The comparison of the results of the material properties of the present sturdy with Ref. [9]

Type of CNT	Epoxy-CNT modulus (GPa)		Longitudinal modulus E_1 (GPa)		Transverse modulus E_2 (GPa)		Shear modulus G_{12} (GPa)		Density (Kg/m^3)	
	Present	Ref.[9]	Present	Ref.[9]	Present	Ref.[9]	Present	Ref.[9]	Present	Ref.[9]
No CNT	2.0000	2.00	23.0000	22.80	4.2909	4.29	1.3826	1.36	1539.00	1532.0
0.5% MWNT	2.1878	2.19	23.1315	22.91	4.6678	4.67	1.5079	1.48	1540.32	1540.0
1.0% MWNT	2.3764	2.37	23.2635	23.02	5.0419	5.04	1.6331	1.60	1541.64	1541.5
1.5% MWNT	2.5656	2.56	23.3959	23.13	5.4133	5.41	1.7579	1.72	1542.97	1543.0
0.5% SWNT	2.1912	2.19	23.1339	22.91	4.6745	4.67	1.5102	1.48	1540.32	1540.0

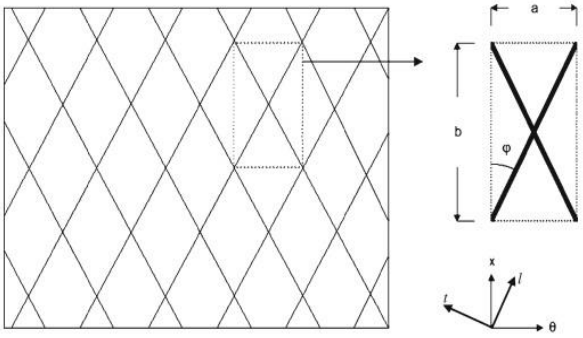

Figure 1. The unit cell and coordinate system for a stiffened cylindrical shell [3]

The strains on the interface of the stiffener and the shell are given by [12]:

$$\begin{aligned}\varepsilon_x &= \varepsilon_x^\circ + \left(\frac{t}{2}\right)\kappa_x \\ \varepsilon_\theta &= \varepsilon_\theta^\circ + \left(\frac{t}{2}\right)\kappa_\theta \\ \varepsilon_{x\theta} &= \varepsilon_{x\theta}^\circ + \left(\frac{t}{2}\right)\kappa_{x\theta}\end{aligned} \tag{6}$$

where $\varepsilon_x^\circ, \varepsilon_\theta^\circ, \varepsilon_{x\theta}^\circ, \kappa_x, \kappa_\theta, \kappa_{x\theta}$ are the mid-plane strains and curvatures of the shell and t is the shell thickness. These strain components should be transformed along the stiffener direction l and t. So the transformation matrix is as what follows [12]:

$$\begin{bmatrix}\varepsilon_l \\ \varepsilon_t \\ \varepsilon_{lt}\end{bmatrix} = \begin{bmatrix} c^2 & s^2 & sc \\ s^2 & c^2 & -sc \\ 2sc & -2sc & s^2-c^2 \end{bmatrix}\begin{bmatrix}\varepsilon_x \\ \varepsilon_\theta \\ \varepsilon_{x\theta}\end{bmatrix} \tag{7}$$

where $c = \cos\varphi, s = \sin\varphi$, and ϕ is the stiffener orientation angle. Fig. 2 shows the force free body diagram on the unit cell. The axial and shear forces in the stiffener direction are expressed as what follows [12]:

$$\begin{aligned} F_{l1} &= E_l A\varepsilon_{lt} = E_l A\left(\varepsilon_x c^2 + \varepsilon_\theta s^2 - \varepsilon_{x\theta} sc\right) \\ F_{l2} &= E_l A\varepsilon_{l2} = E_l A\left(\varepsilon_x s^2 + \varepsilon_\theta c^2 + \varepsilon_{x\theta} sc\right) \\ F_{lt1} &= G_{lt} A\varepsilon_{lt1} = G_{lt} A\left(-2\varepsilon_x sc + 2\varepsilon_\theta sc + \varepsilon_{x\theta}\left(s^2-c^2\right)\right) \\ F_{lt2} &= G_{lt} A\varepsilon_{lt2} = G_{lt} A\left(2\varepsilon_x sc - 2\varepsilon_\theta sc + \varepsilon_{x\theta}\left(s^2-c^2\right)\right) \end{aligned} \tag{8}$$

where E_l and G_{lt} are the longitudinal and shear modulus of the stiffeners, respectively.

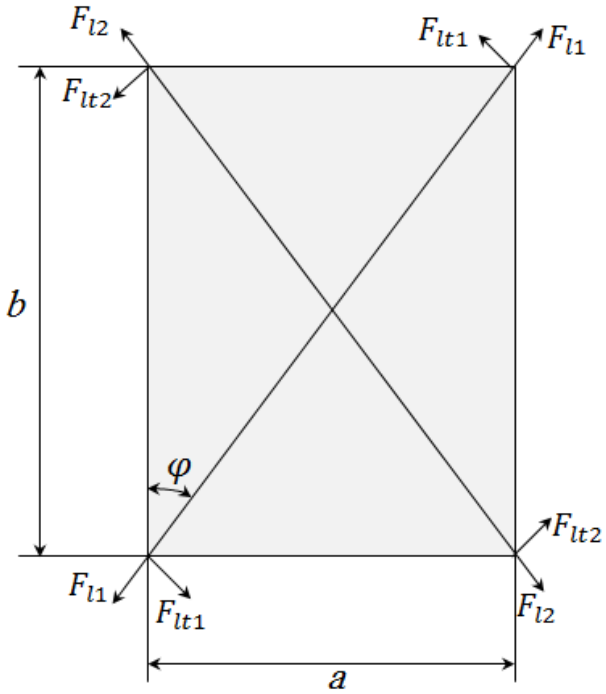

Figure 2. The force distribution on the unit cell [12]

Resolving the axial and shear forces in the x and θ directions, we have the following equations [12]:

$$\begin{aligned} F_x &= \left(F_{l1} + F_{l2}\right)c + \left(F_{lt1} - F_{lt2}\right)s \\ F_\theta &= \left(F_{l1} + F_{l2}\right)s + \left(F_{lt2} - F_{lt1}\right)c \\ F_{x\theta} &= \left(F_{l2} - F_{l1}\right)s + \left(F_{lt1} - F_{lt2}\right)c \end{aligned} \tag{9}$$

Substituting Eqs. (6) and (8) into Eq. (9) and dividing the force expressions by the corresponding edge width of the unit cell, the forces per unit length are carried out as what follow[12]:

$$\begin{aligned} N_x &= \frac{A}{a}\left\{\begin{matrix}\left(2E_l c^3 - 4Gcs^2\right)\varepsilon_x^\circ + \left(2E_l + 4G\right)cs^2\varepsilon_\theta^\circ + \\ \left(E_l c^3 - 2Gcs^2\right)t\kappa_x + \left(E_l + 2G\right)cs^2 t\kappa_\theta\end{matrix}\right\} \\ N_\theta &= \frac{A}{b}\left\{\begin{matrix}\left(2E_l sc^2 + 4Gsc^2\right)\varepsilon_x^\circ + \left(2E_l s^3 - 4Gsc^2\right)\varepsilon_\theta^\circ + \\ \left(E_l sc^2 + 2Gsc^2\right)t\kappa_x + \left(E_l s^3 - 2Gsc^2\right)t\kappa_\theta\end{matrix}\right\} \\ N_{x\theta} &= \frac{A}{a}\left\{\begin{matrix}\left(2E_l cs^2 - 2Gc^3 + 2Gcs^2\right)\varepsilon_{x\theta}^\circ \\ +\left(E_l cs^2 - Gc^3 + Gcs^2\right)\end{matrix}\right\}t\kappa_{x\theta} \end{aligned} \tag{10}$$

According to the shear forces between stiffeners and shell, the torsion and bending moments are

applied to stiffeners and shell. Fig. 3 shows the moments free body diagram which is applied to unit cell. Then, the same as before, the resultant moments can be obtained as what follows [12]:

$$M_x = \frac{A}{a}\begin{Bmatrix}\left(E_l - 2G\right)sc^2t\,\varepsilon_x^{\circ} + \left(E_l s^3 + 2Gsc^2\right)t\,\varepsilon_\theta^{\circ} + \\ \frac{1}{2}\left(E_1 - G\right)sc^2t^2\kappa_x + \left(E_l + Gsc^2\right)t^2\kappa_\theta\end{Bmatrix}$$

$$M_\theta = \frac{A}{b}\begin{Bmatrix}\left(E_l + 2G\right)sc^2t\,\varepsilon_x^{\circ} + \left(E_l s^3 - 2Gsc^2\right)t\,\varepsilon_\theta^{\circ} + \\ \frac{1}{2}\left(E_l + 2G\right)sc^2t^2\kappa_x + \frac{1}{2}\left(E_l s^3 - 2Gsc^2\right)t^2\kappa_\theta\end{Bmatrix} \quad (11)$$

$$M_{x\theta} = \frac{A}{a}\begin{Bmatrix}\left(E_l cs^2 - 2Gc^3 + 2Gcs^2\right)t\,\varepsilon_{x\theta}^{\circ} + \\ \frac{1}{2}\left(E_l cs^2 + Gc^3 - Gcs^2\right)t^2\kappa_{x\theta}\end{Bmatrix}$$

Fig. 4 shows the transverse shear forces, and the strain components are as what follows [12]:

$$\begin{bmatrix}\gamma_{lz}\\ \gamma_{tz}\end{bmatrix} = \begin{bmatrix}c & s\\ -s & c\end{bmatrix}\begin{bmatrix}\varepsilon_{xz}\\ \varepsilon_{\theta z}\end{bmatrix} \quad (12)$$

where $\varepsilon_{lz}, \varepsilon_{tz}$ are the transverse shear strains in the stiffeners, and $\varepsilon_{xz}, \varepsilon_{\theta z}$ are the transverse shear strains in the shell. Then, the shear forces resulting from the shear strains are given as the following expressions [12]:

$$F_{lz}^1 = GA\varepsilon_{lz}^1 = GA\left(\varepsilon_{xz}c - \varepsilon_{\theta z}s\right)$$
$$F_{lz}^2 = GA\varepsilon_{lz}^2 = GA\left(\varepsilon_{xz}c + \varepsilon_{\theta z}s\right) \quad (13)$$

Rewriting these forces in the x and θ directions, we have the following equations [12]:

$$Q_x = \frac{1}{a}\left(F_{lz}^1 + F_{lz}^2\right)$$
$$Q_\theta = \frac{1}{b}\left(F_{lz}^2 - F_{lz}^1\right) \quad (14)$$

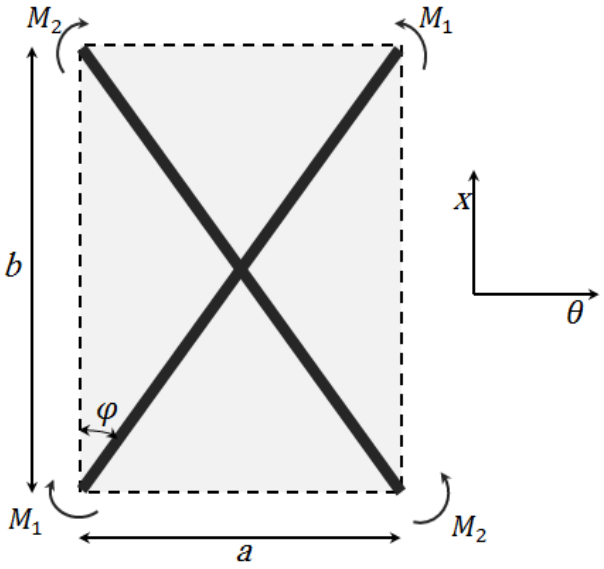

Figure 3. The moments free body diagram on the unit cell [12]

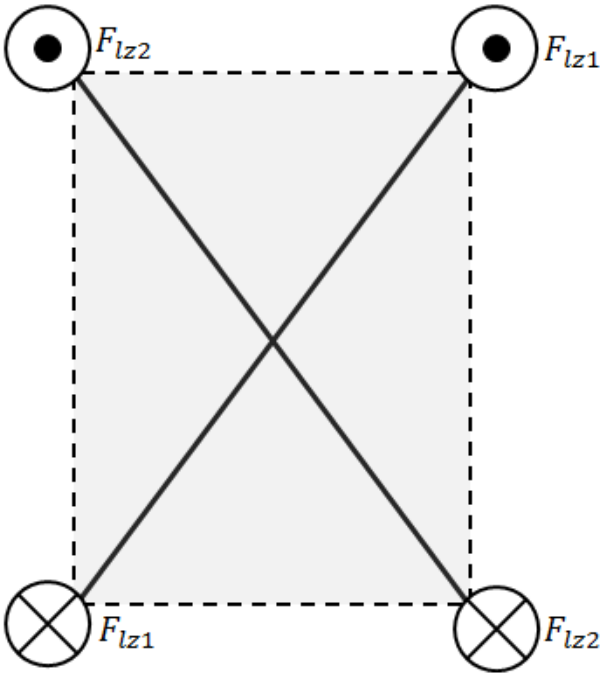

Figure 4. The transverse shear forces [12]

The resultant shear forces per unit length can be obtained by dividing the above forces by the corresponding length are what follows [12]:

$$\left[A_s^{st}\right] = \begin{bmatrix}\frac{2G_{lz}Ac}{b} & 0\\ 0 & \frac{2G_{lz}As}{a}\end{bmatrix} \quad (15)$$

Therefore, the A^{st}, B^{st}, D^{st} matrices for the stiffeners are expressed as the following [12]:

$$A^{st} = \begin{bmatrix}\frac{2E_1c^3 - 4Gcs^2}{a}A & \frac{2E_1cs^2 + 4Gcs^2}{a}A & 0\\ \frac{2E_1sc^2 + 4Gsc^2}{b}A & \frac{2E_1s^3 - 4Gsc^2}{b}A & 0\\ 0 & 0 & \frac{2E_1cs^2 - 2G\left(c^2 - s^2\right)c}{a}A\end{bmatrix}$$

$$B^{st} = \begin{bmatrix}\frac{E_1c^3 - 2Gcs^2}{a}tA & \frac{E_1cs^2 + 2Gcs^2}{a}tA & 0\\ \frac{E_1sc^2 + 2Gsc^2}{b}tA & \frac{E_1s^3 - 2Gsc^2}{b}tA & 0\\ 0 & 0 & \frac{E_1cs^2 - G\left(c^2 - s^2\right)c}{a}tA\end{bmatrix} \quad (16)$$

$$D^{st} = \begin{bmatrix}\frac{E_1sc^2 - 2Gsc^2}{2a}t^2A & \frac{E_1s^3 + 2Gsc^2}{2a}t^2A & 0\\ \frac{E_1sc^2 + 2Gsc^2}{2b}t^2A & \frac{E_1s^3 - 2Gsc^2}{2b}t^2A & 0\\ 0 & 0 & \frac{E_1cs^2 - G\left(c^2 - s^2\right)c}{2a}t^2A\end{bmatrix}$$

$$\left[A_s^{st}\right] = \begin{bmatrix}\frac{2G_{lz}Ac}{b} & 0\\ 0 & \frac{2G_{lz}As}{a}\end{bmatrix}$$

Also, the resultant force and moments can be written as following (due to the shell in terms of the strain components of the mid-plane surface of the shell) [12].

$$\begin{bmatrix} N \\ M \\ Q \end{bmatrix} = \begin{bmatrix} \left[A^{sh}\right] & \left[B^{sh}\right] & 0 \\ \left[B^{sh}\right] & \left[D^{sh}\right] & 0 \\ 0 & 0 & \left[A_s^{sh}\right] \end{bmatrix} \begin{bmatrix} \varepsilon^{\circ} \\ \kappa \\ \gamma \end{bmatrix} \tag{17}$$

The total force and moment on the structure are the superposition of the forces and moments due to the stiffeners and the shell according to their volume fractions as what follows [12]:

$$\begin{bmatrix} N \\ M \\ Q \end{bmatrix} = \begin{bmatrix} v^{sh}\left[A^{sh}\right]+v^{st}\left[A^{st}\right] & v^{sh}\left[B^{sh}\right]+v^{st}\left[B^{st}\right] & 0 \\ v^{sh}\left[B^{sh}\right]+v^{st}\left[B^{st}\right] & v^{sh}\left[D^{sh}\right]+v^{st}\left[D^{st}\right] & 0 \\ 0 & 0 & v^{sh}\left[A_s^{st}\right]+v^{st}\left[A_s^{st}\right] \end{bmatrix} \begin{bmatrix} \varepsilon^{\circ} \\ \kappa \\ \gamma \end{bmatrix} \tag{18}$$

where v^{st} and v^{sh} are the volume fractions of the stiffener and the shell respectively.

4. Analytical Solution

In First-order Shear Deformation Theory (FSDT), it is assumed that the transverse normal does not remain perpendicular to the mid surface after the deformation, so the displacement fields are as what follows [13]:

$$\begin{aligned} u(x,\theta,z,t) &= u_0(x,\theta,t)+z\,\phi_x(x,\theta,t) \\ v(x,\theta,z,t) &= v_0(x,\theta,t)+z\,\phi_\theta(x,\theta,t) \\ w(x,\theta,z,t) &= w_0(x,\theta,t) \end{aligned} \tag{19}$$

Based on (FSDT), the equilibrium equations for a cylindrical shell are as the following equations [3]:

$$\begin{aligned} &\frac{\partial N_x}{\partial x}+\frac{1}{R}\frac{\partial N_{x\theta}}{\partial \theta} = I_1\frac{\partial^2 u}{\partial t^2}+I_2\frac{\partial^2 \phi_x}{\partial t^2} \\ &\frac{\partial N_{x\theta}}{\partial x}+\frac{1}{R}\frac{\partial N_{\theta}}{\partial \theta} = I_1\frac{\partial^2 v}{\partial t^2}+I_2\frac{\partial^2 \phi_\theta}{\partial t^2} \\ &\frac{\partial Q_x}{\partial x}+\frac{1}{R}\frac{\partial Q_\theta}{\partial \theta}-\frac{N_\theta}{R} = I_1\frac{\partial^2 w}{\partial t^2} \\ &\frac{\partial M_x}{\partial x}+\frac{1}{R}\frac{\partial M_{x\theta}}{\partial \theta}-Q_x = I_3\frac{\partial^2 \phi_x}{\partial t^2}+I_2\frac{\partial^2 u}{\partial t^2} \\ &\frac{\partial M_{x\theta}}{\partial x}+\frac{1}{R}\frac{\partial M_{\theta}}{\partial \theta}-Q_\theta = I_3\frac{\partial^2 \phi_\theta}{\partial t^2}+I_2\frac{\partial^2 v}{\partial t^2} \end{aligned} \tag{20}$$

In the above equation, ϕ_x and ϕ_θ are the slope in the plane of $(x-z)$ and $(\phi-z)$ respectively.

I_1, I_2, I_3 are defined by the following relation [3]:

$$(I_1, I_2, I_3) = \int_{\frac{-t}{2}}^{\frac{t}{2}} \rho_{(k)}\left(1, z, z^2\right)dz \tag{21}$$

where $\rho_{(k)}$ is the density for each layer. Moreover, the stiffness of the shell is given by the following expressions [2]:

$$\begin{aligned} \begin{bmatrix} N_x \\ N_\theta \\ N_{x\theta} \end{bmatrix} &= \begin{bmatrix} A_{11} & A_{12} & A_{16} \\ A_{12} & A_{22} & A_{26} \\ A_{16} & A_{26} & A_{66} \end{bmatrix} \begin{bmatrix} \varepsilon_x^{\circ} \\ \varepsilon_\theta^{\circ} \\ \gamma_{x\theta}^{\circ} \end{bmatrix} + \begin{bmatrix} B_{11} & B_{12} & B_{16} \\ B_{12} & B_{22} & B_{26} \\ B_{16} & B_{26} & B_{66} \end{bmatrix} \begin{bmatrix} \kappa_x^{\circ} \\ \kappa_\theta^{\circ} \\ \kappa_{x\theta}^{\circ} \end{bmatrix} \\ \begin{bmatrix} M_x \\ M_\theta \\ M_{x\theta} \end{bmatrix} &= \begin{bmatrix} B_{11} & B_{12} & B_{16} \\ B_{12} & B_{22} & B_{26} \\ B_{16} & B_{26} & B_{66} \end{bmatrix} \begin{bmatrix} \varepsilon_x^{\circ} \\ \varepsilon_\theta^{\circ} \\ \gamma_{x\theta}^{\circ} \end{bmatrix} + \begin{bmatrix} D_{11} & D_{12} & D_{16} \\ D_{12} & D_{22} & D_{26} \\ D_{16} & D_{26} & D_{66} \end{bmatrix} \begin{bmatrix} \kappa_x^{\circ} \\ \kappa_\theta^{\circ} \\ \kappa_{x\theta}^{\circ} \end{bmatrix} \\ \begin{bmatrix} Q_x \\ Q_\theta \end{bmatrix} &= \begin{bmatrix} H_{55} & H_{45} \\ H_{45} & H_{44} \end{bmatrix} \begin{bmatrix} \gamma_{xz}^{\circ} \\ \gamma_{\theta z}^{\circ} \end{bmatrix} \end{aligned} \tag{22}$$

where A, B, D and H are the extensional, coupling, bending and thickness shear stiffness matrices respectively and they are defined as what follows [2]:

$$\begin{aligned} &(A_{ij}, B_{ij}, D_{ij}) = \int_{\frac{-h}{2}}^{\frac{h}{2}} \left(1, Z, Z^2\right)\overline{Q}_{ij}dz \qquad (i,j=1,2,6) \\ &H_{ij} = K_{\circ}\int_{\frac{-h}{2}}^{\frac{h}{2}} \left(1, Z, Z^2\right)\overline{Q}_{ij}dz \qquad (i,j=4,5) \end{aligned} \tag{23}$$

where $K_{\circ}$ is the shear correction factor and equals to $\pi^2/12$ [2]. The mid plane strain and curvature components are given by the following equations [2]:

$$\begin{aligned} \begin{Bmatrix} \varepsilon_x^{\circ} \\ \varepsilon_\theta^{\circ} \\ \gamma_{x\theta}^{\circ} \end{Bmatrix} &= \begin{Bmatrix} \dfrac{\partial u}{\partial x} \\ \dfrac{1}{R}\dfrac{\partial v}{\partial \theta}+\dfrac{W}{R} \\ \dfrac{1}{R}\dfrac{\partial u}{\partial \theta}+\dfrac{\partial v}{\partial x} \end{Bmatrix}, \qquad \begin{Bmatrix} \kappa_x^{\circ} \\ \kappa_\theta^{\circ} \\ \kappa_{x\theta}^{\circ} \end{Bmatrix} = \begin{Bmatrix} \dfrac{\partial \phi_x}{\partial x} \\ \dfrac{1}{R}\dfrac{\partial \phi_\theta}{\partial \theta} \\ \dfrac{1}{R}\dfrac{\partial \phi_x}{\partial \theta}+\dfrac{\partial \phi_\theta}{\partial x} \end{Bmatrix} \\ \begin{Bmatrix} \gamma_{xz}^{\circ} \\ \gamma_{\theta z}^{\circ} \end{Bmatrix} &= \begin{Bmatrix} \phi_x+\dfrac{\partial w}{\partial x} \\ \phi_\theta+\dfrac{1}{R}\dfrac{\partial w}{\partial \theta}-\dfrac{v}{R} \end{Bmatrix} \end{aligned} \tag{24}$$

The boundary conditions for the cylindrical shell which are simply supported along its curved edges at $x=0$ and $x=L$ are considered as what follows [2]:

$$\begin{aligned} &N_x(0,\theta,t) = N_x(L,\theta,t) = 0 \\ &M_x(0,\theta,t) = M_x(L,\theta,t) = 0 \\ &W(0,\theta,t) = W(L,\theta,t) = 0 \\ &V(0,\theta,t) = V(L,\theta,t) = 0 \\ &\phi_\theta(0,\theta,t) = \phi_\theta(L,\theta,t) = 0 \end{aligned} \tag{25}$$

The following functions are assumed to satisfy the simply-supported boundary conditions and the equations of motion:

$$u(x,\theta,t)=\sum_{m=1}^{\infty}\sum_{n=1}^{\infty}U_{mn}\cos(\alpha x)\sin(n\theta)\sin(\omega t)$$
$$v(x,\theta,t)=\sum_{m=1}^{\infty}\sum_{n=1}^{\infty}V_{mn}\sin(\alpha x)\cos(n\theta)\sin(\omega t)$$
$$w(x,\theta,t)=\sum_{m=1}^{\infty}\sum_{n=1}^{\infty}W_{mn}\sin(\alpha x)\sin(n\theta)\sin(\omega t) \quad (26)$$
$$\phi_x(x,\theta,t)=\sum_{m=1}^{\infty}\sum_{n=1}^{\infty}X_{mn}\cos(\alpha x)\sin(n\theta)\sin(\omega t)$$
$$\phi_\theta(x,\theta,t)=\sum_{m=1}^{\infty}\sum_{n=1}^{\infty}Y_{mn}\sin(\alpha x)\cos(n\theta)\sin(\omega t)$$

Now, substituting Eq. (24) into Eq. (22) and then enforcing the result into Eq. (20), the free vibration Eigen-equations yield to what follows:

$$([C]-\omega^2[M])U=0 \quad (27)$$

$$U=\{U_{mn},V_{mn},W_{mn},X_{mn},Y_{mn}\}^T \quad (28)$$

where $[C]$ and $[M]$ are stiffness and mass matrices respectively and are shown in appendix.

5. Results

The geometry of the structure is shown in Table 2. Two types of L/D are considered. The cylindrical shell is assumed to be [45/-45/45/-45/45] stacking sequence, while in the stiffener structure, the fibers are considered to be oriented in the ribs' directions. It is supposed that the CNTs have randomly orientation for both the single-wall and multi-wall CNTs. The material properties of the glass fiber, carbon nano-tubes and epoxy resin are given as what follows:

$E_f=72Gpa$ $E_{CNT}=900Gpa$ $G_f=30.1Gpa$
$G_{23}=1.34Gpa$ $\upsilon_m=0.3$ $\upsilon_f=0.2$
$\rho_m=1110\ Kg/m^3$ $\rho_f=2540\ Kg/m^3$ $\rho_{CNT}=1680\ Kg/m^3$
$d_{MWNT}=15nm$ $d_{SWNT}=2.5nm$ $K_w=0.4$
$\%W_{CNT}=0,1,2,3$ $E_m=2Gpa$ $V_f=0.5$
$\alpha=1/6$ $l=10\mu m$

The boundary conditions are applied in both edges of the cylinder in the ABAQUS software. The structure is fixed in both the circumferential and thickness directions and is free in the longitudinal direction. Also, the M_x is fixed, too. The number of the elements is about 475395 and their types are structured ones for the lattice cylinder and the shell sweep for the cylindrical shell. Table 3 and Table 4 show a comparison of the first five natural frequencies got via analytical solution and FEM approach in two types of the length to diameter ratio (L/D = 1 and 2) and the carbon nano-tubes (MWNT and SWNT).

A good agreement has been seen among the results and the maximum error is less than 10%. As shown in Fig. 5, it is clear that with an increase in the weight fraction of the CNTs, the natural frequency of the structure increases linearly.

Figs. 6 and 7 give the first five mode shapes of the lattice cylindrical shell in L/D = 1 and 2 ratios, respectively.

Tables 5, 6 and 7 give a comparison of different rib angles. Three kinds of the rib angle are chosen (30°, 35° and 40°) to investigate the effect of the rib orientation on the natural frequency of the structure.

Fig. 8 shows the natural frequency decreases at first and then by enhancing the amount of rib angle, it increases.

Table 2. Geometrical parameters of the lattice cylindrical shell

Shell height (mm)	For L/D = 1, L = 240 For L/D = 2, L = 480
Diameter (mm)	For L/D = 1, D = 240 For L/D = 2, D = 242.584
Shell thickness (mm)	3
Helical rib distance, a_k (mm)	60
Stiffener orientation (ϕ°)	±30
Stiffener thickness (mm)	3
Stiffener width (mm)	5

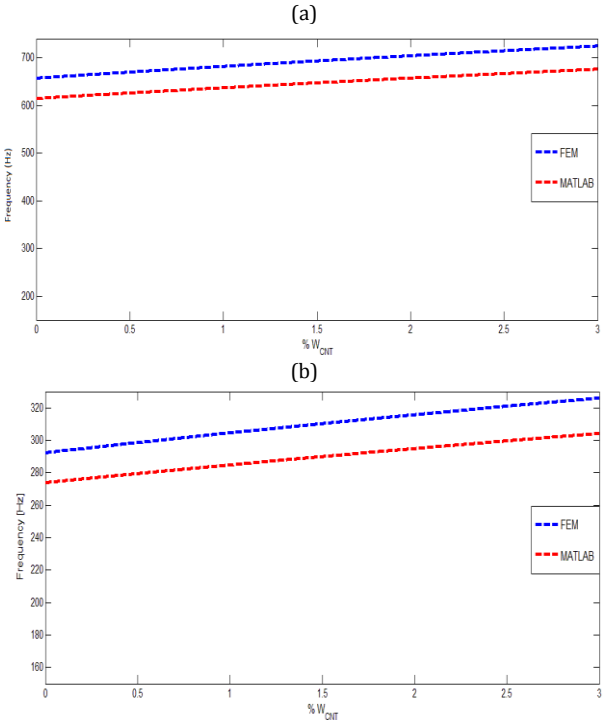

Figure 5. Variations of the natural frequencies with different weight fractions of the CNTs; (a) L/D = 1 and (b) L/D = 2

Table 3. Natural frequencies of the lattice cylindrical shell reinforced with the glass fiber and MWNT

$\frac{L}{D}$	m	n	$\%W_{CNT}=0$			$\%W_{CNT}=1$		
			Analytical (Hz)	FEM (Hz)	Difference %	Analytical (Hz)	FEM (Hz)	Difference %
	1	4	614.05	656.58	6.92	636.37	681.23	7.05
	1	5	737.56	793.78	7.62	758.43	819.58	8.06
1	1	3	743.94	801.15	7.69	776.34	832.58	7.24
	1	6	974.71	1050.30	7.76	1000.73	1084.4	8.36
	1	7	1275.89	1373.40	7.64	1310.39	1419.5	8.33
	1	3	273.72	292.12	6.72	284.65	304.38	6.93
	1	2	366.17	401.44	9.63	386.81	421.75	9.03
2	1	4	397.72	430.49	8.24	409.34	445.05	8.72
	2	4	606.09	656.71	8.35	623.29	679.43	9.01
	1	5	614.05	658.73	7.28	636.37	683.69	7.44

Continued Table 4 Natural frequencies of the lattice cylindrical shell reinforced with the glass fiber and MWNT

$\frac{L}{D}$	m	n	$\%W_{CNT}=2$		$\%W_{CNT}=3$			
			Analytical (Hz)	FEM (Hz)	Analytical (Hz)	FEM (Hz)	Analytical (Hz)	FEM (Hz)
	1	4	656.69	703.56	656.69	703.56	656.69	703.56
	1	5	778.02	843.36	778.02	843.36	778.02	843.36
1	1	3	804.74	860.36	804.74	860.36	804.74	860.36
	1	6	1025.36	1116	1025.36	1116	1025.36	1116
	1	7	1343.12	1462	1343.12	1462	1343.12	1462
	1	3	294.71	315.57	294.71	315.57	294.71	315.57
	1	2	405.05	439.76	405.05	439.76	405.05	439.76
2	1	4	420.31	458.55	420.31	458.55	420.31	458.55
	2	4	639.63	700.46	639.63	700.46	639.63	700.46
	1	5	656.69	706.27	656.69	706.27	656.69	706.27

Table 5. Natural frequencies of the lattice cylindrical shell reinforced with the glass fiber and SWNT

$\frac{L}{D}$	m	n	$\%W_{CNT}=0$		$\%W_{CNT}=1$			
			Analytical (Hz)	FEM (Hz)	Analytical (Hz)	FEM (Hz)	Analytical (Hz)	FEM (Hz)
	1	4	614.05	656.58	614.05	656.58	614.05	656.58
	1	5	737.56	793.78	737.56	793.78	737.56	793.78
1	1	3	743.94	801.15	743.94	801.15	743.94	801.15
	1	6	974.71	1050.30	974.71	1050.30	974.71	1050.30
	1	7	1275.89	1373.40	1275.89	1373.40	1275.89	1373.40
	1	3	273.72	292.12	273.72	292.12	273.72	292.12
	1	2	366.17	401.44	366.17	401.44	366.17	401.44
2	1	4	397.72	430.49	397.72	430.49	397.72	430.49
	2	4	606.09	656.71	606.09	656.71	606.09	656.71
	1	5	614.05	658.73	614.05	658.73	614.05	658.73

Continued Table 6. Natural frequencies of the lattice cylindrical shell reinforced with the glass fiber and SWNT

$\frac{L}{D}$	m	n	$\%W_{CNT}=2$		$\%W_{CNT}=3$			
			Analytical (Hz)	FEM (Hz)	Analytical (Hz)	FEM (Hz)	Analytical (Hz)	FEM (Hz)
	1	4	657.39	704.32	657.39	704.32	657.39	704.32
	1	5	778.70	844.19	778.70	844.19	778.70	844.19
1	1	3	805.69	861.31	805.69	861.31	805.69	861.31
	1	6	1026.23	1117.10	1026.23	1117.10	1026.23	1117.10
	1	7	1344.27	1463.50	1344.27	1463.50	1344.27	1463.50
	1	3	295.05	315.95	295.05	315.95	295.05	315.95
	1	2	405.67	440.37	405.67	440.37	405.67	440.37
2	1	4	420.69	459.02	420.69	459.02	420.69	459.02
	2	4	640.20	701.19	640.20	701.19	640.20	701.19
	1	5	657.39	707.04	657.39	707.04	657.39	707.04

(a) 1st Mode (*m*=1,n=*4*)

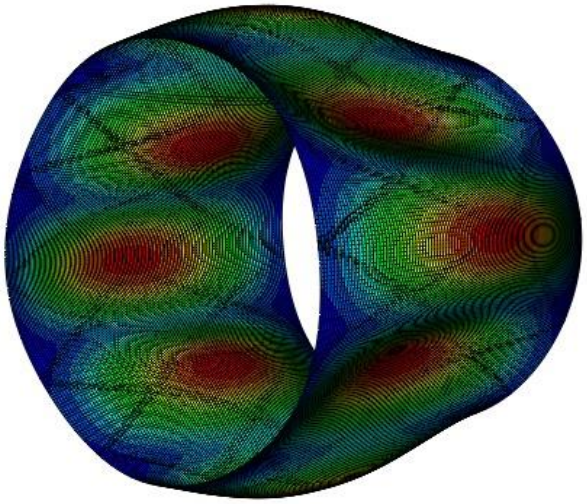

(b) 2nd Mode (*m*=1,*n*=5)

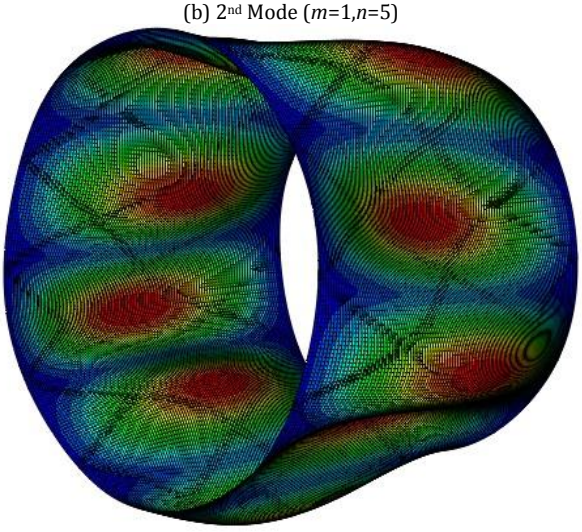

(c) 3rd Mode (*m*=1,*n*=3)

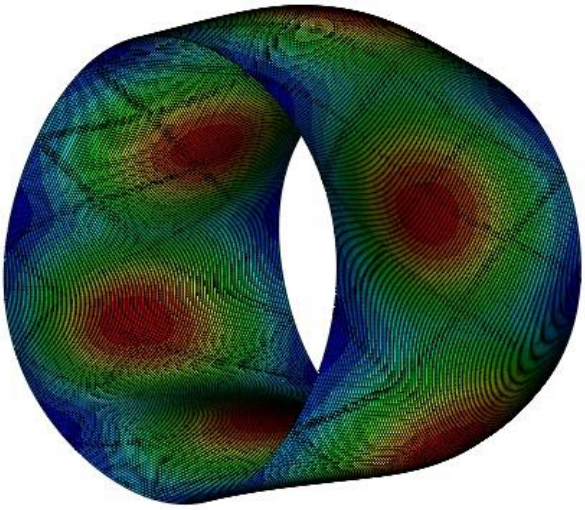

(d) 4th Mode (*m*=1,*n*=6)

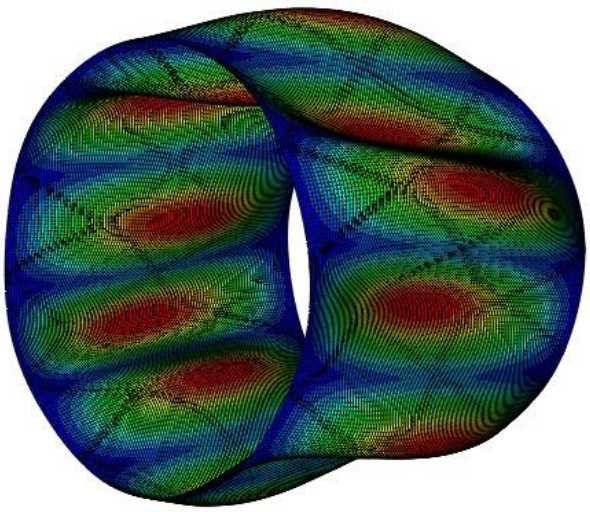

(e) 5th Mode (*m*=1,*n*=7)

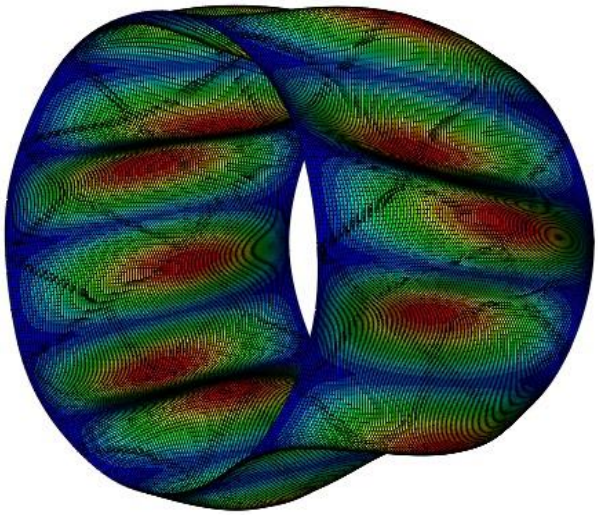

Figure 6. The mode shapes of the lattice cylindrical shell with L/D = 1

(a) 1st Mode (*m*=1,*n*=3)

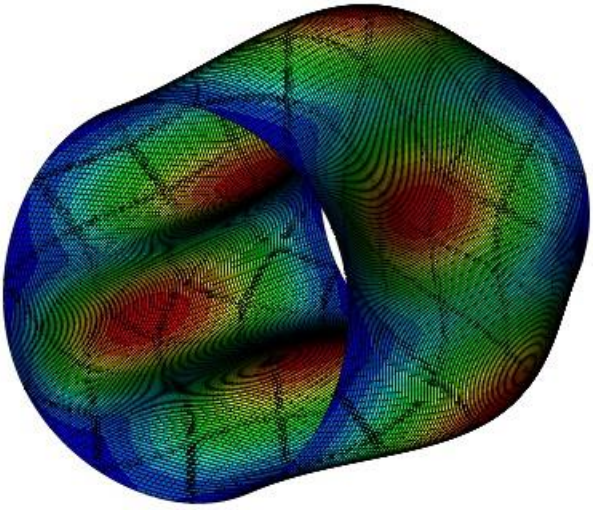

(b) 2nd Mode (*m*=1,*n*=2)

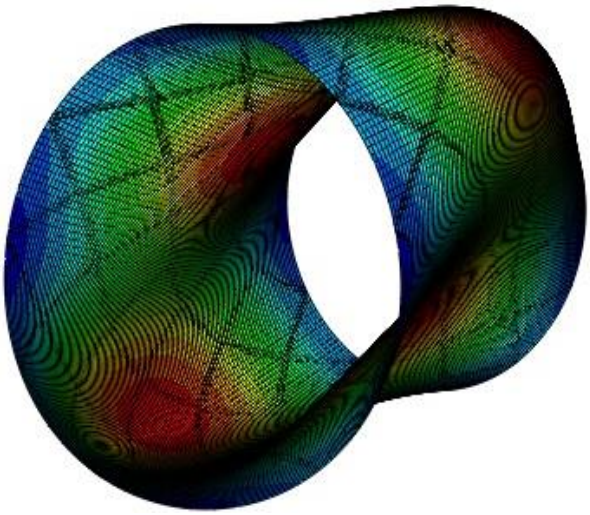

(c) 3rd Mode (*m*=1,*n*=4)

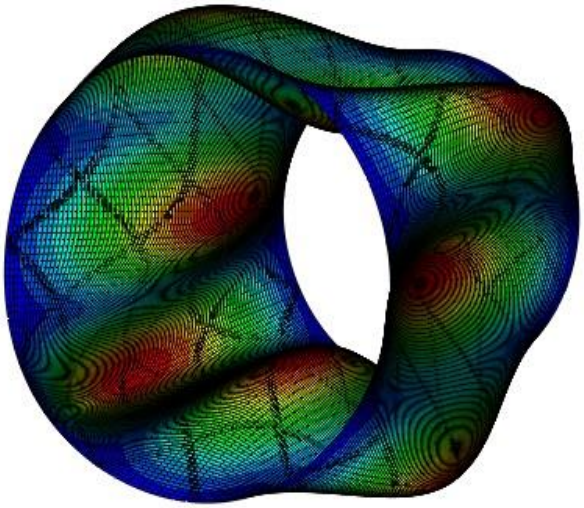

(d) 4th Mode (*m*=2,*n*=4)

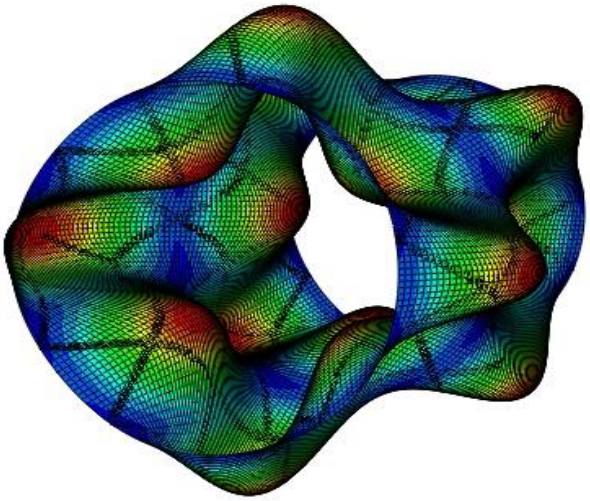

(e) 5th Mode (*m*=1,*n*=5)

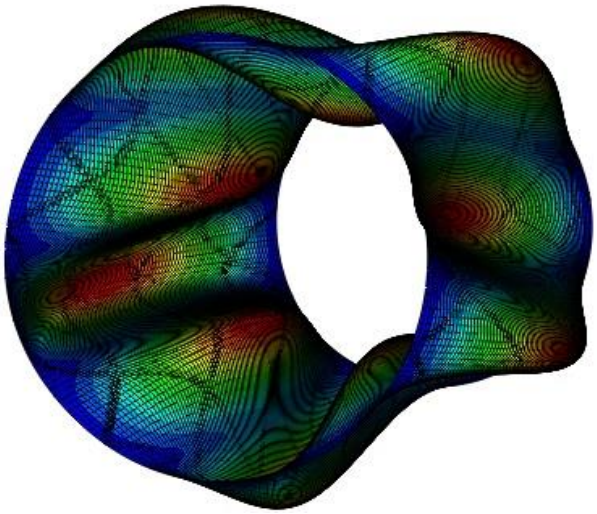

Figure 7. The mode shapes of the lattice cylindrical shell with L/D = 2

Table 7. Non-dimension natural frequencies of the lattice cylindrical shell reinforced with the multi-wall CNTs and rib angle of 30°

$\frac{L}{D}$	m	n	$\%W_{CNT}=0$				$\%W_{CNT}=1$	
			Analytical (Hz)	FEM (Hz)	Analytical (Hz)	FEM (Hz)	Analytical (Hz)	FEM (Hz)
	1	3	0.0463	0.0494	6.70	0.0481	0.0514	6.86
	1	2	0.0620	0.0679	9.52	0.0653	0.0712	9.04
2	1	4	0.0673	0.0729	8.32	0.0691	0.0752	8.83
	2	4	0.1026	0.1112	8.38	0.1053	0.1148	9.02
	1	5	0.1039	0.1115	7.31	0.1075	0.1155	7.44

Continued Table 8. Non-dimension natural frequencies of the lattice cylindrical shell reinforced with the multi-wall CNTs and rib angle of 30°

$\frac{L}{D}$	m	n	$\%W_{CNT}=2$				$\%W_{CNT}=3$	
			Analytical (Hz)	FEM (Hz)	Analytical (Hz)	FEM (Hz)	Analytical (Hz)	FEM (Hz)
	1	3	0.0497	0.0532	7.04	0.0511	0.0548	7.24
	1	2	0.0683	0.0741	8.49	0.0709	0.0767	8.18
2	1	4	0.0709	0.0773	9.03	0.0725	0.0793	9.38
	2	4	0.1078	0.1181	9.55	0.1102	0.1211	9.89
	1	5	0.1107	0.1191	7.59	0.1136	0.1223	7.66

Table 9. Non-dimension natural frequencies of the lattice cylindrical shell reinforced with the multi-wall CNTs and rib angle of 35°

$\frac{L}{D}$	m	n	$\%W_{CNT}=0$				$\%W_{CNT}=1$	
			Analytical (Hz)	FEM (Hz)	Analytical (Hz)	FEM (Hz)	Analytical (Hz)	FEM (Hz)
	1	3	0.0435	0.0465	6.90	0.0452	0.0483	6.86
	1	2	0.0578	0.0623	7.79	0.0611	0.0656	7.36
2	1	4	0.0636	0.0697	9.59	0.0654	0.0718	9.79
	2	4	0.0972	0.1045	7.51	0.0998	0.1084	8.62
	1	5	0.0972	0.1066	9.67	0.1006	0.1100	9.34

Continued Table 10. Non-dimension natural frequencies of the lattice cylindrical shell reinforced with the multi-wall CNTs and rib angle of 35°

$\frac{L}{D}$	m	n	$\%W_{CNT}=2$				$\%W_{CNT}=3$	
			Analytical (Hz)	FEM (Hz)	Analytical (Hz)	FEM (Hz)	Analytical (Hz)	FEM (Hz)
	1	3	0.0467	0.0500	7.07	0.0481	0.0516	7.28
	1	2	0.0639	0.0685	7.20	0.0664	0.0710	6.93
2	1	4	0.0670	0.0738	10.15	0.0685	0.0756	10.36
	2	4	0.1022	0.1118	9.39	0.1044	0.1149	10.06
	1	5	0.1037	0.1131	9.06	0.1065	0.1160	8.92

Table 11. Non-dimension natural frequencies of the lattice cylindrical shell reinforced with the multi-wall CNTs and rib angle of 40°

$\frac{L}{D}$	m	n	$\%W_{CNT}=0$				$\%W_{CNT}=1$	
			Analytical (Hz)	FEM (Hz)	Analytical (Hz)	FEM (Hz)	Analytical (Hz)	FEM (Hz)
	1	3	0.0469	0.0504	7.46	0.0487	0.0524	7.60
	1	2	0.0560	0.0639	14.11	0.0633	0.0674	6.48
2	1	4	0.0701	0.0772	10.13	0.0720	0.0796	10.5
	2	4	0.1048	0.1133	8.11	0.1083	0.1172	8.22
	1	5	0.1074	0.1182	10.06	0.1102	0.1219	10.6

Continued Table 12. Non-dimension natural frequencies of the lattice cylindrical shell reinforced with the multi-wall CNTs and rib angle of 40°

$\frac{L}{D}$	m	n	$\%W_{CNT}=2$				$\%W_{CNT}=3$	
			Analytical (Hz)	FEM (Hz)	Analytical (Hz)	FEM (Hz)	Analytical (Hz)	FEM (Hz)
	1	3	0.0503	0.0541	7.55	0.0518	0.0558	7.72
	1	2	0.0663	0.0705	6.33	0.0689	0.0732	6.24
2	1	4	0.0737	0.0817	10.8	0.0754	0.0837	11.01
	2	4	0.1116	0.1208	8.24	0.1145	0.1240	8.30
	1	5	0.1128	0.1252	10.9	0.1152	0.1284	11.46

Since the design of the lattice cylindrical shell with different rib angles in a specific length to diameter ratio has some limitations, the effect of weight should be omitted using Eq. (27) [14]. The main reason of this behavior can only be described in changing the structure stiffness.

$$\bar{\omega} = \omega R \sqrt{\frac{\rho}{E_1}} \tag{27}$$

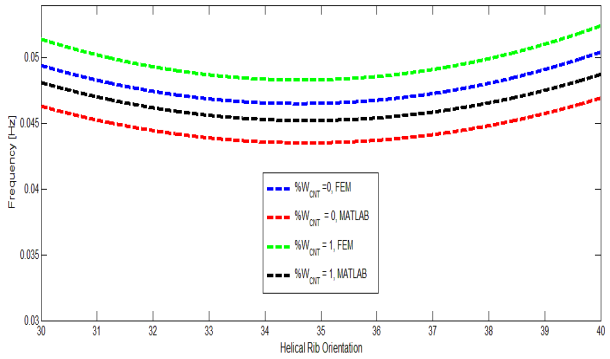

Figure 8. Variations of the non-dimensional natural frequency of the lattice cylindrical shell reinforced with the MWNT nano-tubes in different rib angles of 30°, 35° and 40°

6. Conclusion

The free vibrations of the lattice cylindrical shell reinforced with the carbon nano-tubes are investigated. The analytical method is based on First-order Shear Deformation Theory (FSDT). According to the smeared method, the equivalent stiffness of the structure was calculated and then it was entered into the analytical procedure to find the natural frequencies. In order to find out the material properties of a composite reinforced with CNTs, the modified Halpin-Tsai equations were used. The analytical results are validated by the FEM results and a good agreement has been observed. It can be understood from the results that adding CNTs increases the natural frequency linearly. Besides, by changing the rib angle, the stiffness of the structure changes, too. First, the natural frequency decreases and then it increases.

Nomenclature

E_{em}, G_{em}	Young's and shear modulus of modified polymer reinforced with CNTs
K_w	Waviness factor
α	Orientation parameter
$\varepsilon_i \ (i = x, \theta, x\theta)$	Mid plane strains
$\kappa_i \ (i = x, \theta, x\theta)$	Mid plane curvatures
$\gamma_i \ (i = xz, \theta z)$	Transverse shear strain
ϕ_x	Slope in the plane of $x-z$
ϕ_θ	Slope in the plane of $\theta-z$
I_1, I_2, I_3	Mass inertia
W_{CNT}	Weight fraction of CNTs
$K_\circ$	Shear correction factor
V_f	Volume fraction of fiber
$\rho_f, \rho_m, \rho_{CNT}$	Density of fiber, polymer and carbon nano-tubes
E_f, E_m, E_{CNT}	Young modulus of fiber, polymer and carbon nano-tubes
υ_f, υ_m	Poisson ratio of fiber and polymer
l	Length of CNT
d_{SWNT}, d_{MWNT}	Diameter of single wall and multi wall nano-tubes
φ	Rib angle

Appendix

Stiffness Coefficients:

$$C_{11} = -A_{11}\alpha^2 - \frac{A_{66}}{R^2}n^2$$

$$C_{12} = -\frac{A_{12}}{R}\alpha n - \frac{A_{66}}{R}\alpha n$$

$$C_{13} = \frac{A_{12}}{R}\alpha$$

$$C_{14} = -B_{11}\alpha^2 - \frac{B_{66}}{R^2}n^2$$

$$C_{15} = -\frac{B_{12}}{R}\alpha n - \frac{B_{66}}{R}\alpha n$$

$$C_{21} = -\frac{A_{12}}{R}\alpha n - \frac{A_{66}}{R}\alpha n$$

$$C_{22} = -A_{66}\alpha^2 - \frac{A_{22}}{R^2}n^2 - \frac{A_{s_{44}}}{R^2}$$

$$C_{23} = \frac{A_{22}}{R^2}n + \frac{A_{s_{44}}}{R^2}n$$

$$C_{24} = -\frac{B_{66}}{R}\alpha n - \frac{B_{12}}{R}\alpha n$$

$$C_{25} = -B_{66}\alpha^2 - \frac{B_{22}}{R^2}n^2 + \frac{A_{s_{44}}}{R}$$

$$C_{31} = C_{13} \quad , \quad C_{32} = C_{23}$$

$$C_{33} = -A_{s_{55}}\alpha^2 - \frac{A_{s_{44}}}{R^2}n^2 - \frac{A_{22}}{R^2}$$

$$C_{34} = -A_{s_{55}}\alpha + \frac{B_{12}}{R}\alpha$$

$$C_{35} = -\frac{A_{s_{44}}}{R}n + \frac{B_{22}}{R^2}n$$

$$C_{41} = -B_{11}\alpha^2 - \frac{B_{66}}{R^2}n^2$$

$$C_{42} = -\frac{B_{66}}{R}\alpha n - \frac{B_{12}}{R}\alpha n$$

$$C_{43} = C_{34}$$

$$C_{44} = -D_{11}\alpha^2 - \frac{D_{66}}{R^2}n^2 - A_{s_{55}}$$

$$C_{45} = -\frac{D_{12}}{R}\alpha n - \frac{D_{66}}{R}\alpha n$$

$$C_{51} = -\frac{B_{12}}{R}\alpha n - \frac{B_{66}}{R}\alpha n$$

$$C_{52} = -B_{66}\alpha^2 - \frac{B_{22}}{R^2}n^2 + \frac{A_{s_{44}}}{R}$$

$$C_{53} = C_{35} \qquad C_{54} = C_{45}$$

$$C_{55} = -D_{66}\alpha^2 - \frac{D_{22}}{R^2}n^2 - A_{s_{44}}$$

Mass Coefficients:

$$M_{11} = \rho h$$

$$M_{22} = \rho h$$

$$M_{33} = \rho h$$

$$M_{44} = \frac{\rho h^3}{12}$$

$$M_{55} = \frac{\rho h^3}{12}$$

References

[1] Vasiliev VV, Barynin VA, Rasin AF. Anisogrid Lattice Structures - Survey of Development and Application. *Compos Struct* 2001; 54: 361–370.

[2] KhaliliS MR, Azarafza R, Davar A. Transient Dynamic Response of Initially Stressed Composite Circular Cylindrical Shells under Radial Impulse Load. *Compos Struct* 2009; 89: 275–284.

[3] Hemmatnezhad M, Rahimi GH, Ansari R. On the Free Vibrations of Grid-stiffened Composite Cylindrical Shells. *Springer* 2014; 225: 609–623.

[4] Zhang H, Sun F, Fan H, Chen H, Chen L, Fang D. Free Vibration Behaviors of Carbon Fiber Reinforced Lattice-core Sandwich Cylinder. *Compos Sci Technol* 2014; 100: 26–33.

[5] Zhu P, Lei ZX, Liew KM. Static and Free Vibration Analyses of Carbon Nano-tube-reinforced Composite Plates using Finite Element Method with First-order Shear Deformation Plate Theory. *Compos Struct* 2012; 94: 1450–1460.

[6] Reddy BR, Ramji K, Satyanarayana B. Free Vibration Analysis of Carbon Nano-tube Reinforced Laminated Composite Panels. *World Acad Sci Eng Technol* 2011; 5: 8–29.

[7] Sobhani Aragh B, Borzabadi Farahani E, Nasrollah Barati AH. Natural Frequency Analysis of Continuously Graded Carbon Nano-tube-reinforced Cylindrical Shells based on Third-order Shear Deformation Theory. *Math Mech Solids* 2013; 18: 264–284.

[8] Arasteh R, Omidi M, Rousta AHA, Kazerooni H. A Study on Effect of Waviness on Mechanical Properties of Multi-Walled Carbon Nano-tube/Epoxy Composites Using Modified Halpin–Tsai Theory. *J Macromolecular Sci Part: B Physics* 2011; 50(12): 2464–2480.

[9] Asadi E. **Manufacturing and Experimental Study of Vibration of Laminated Composite Plates Reinforced by Carbon Nano-tube**. MSc Thesis, Malek-Ashtar Uuniversity of Technology, Iran, 2013.

[10] Kidane S, Li G, Helms J, Pang S, Woldesenbet E. Buckling Load Analysis of Grid Stiffened Composite Cylinders. *Compos* 2003; 34: 1–9.

[11] Wodesenbet E, Kidane S, Pang S. Optimization for Buckling Loads of Grid Stiffened Composite Panels. *Compos* 2003; 60: 159–169.

[12] Ghasemi MA, Yazdani M, Hoseini SM. Analysis of Effective Parameters on the Buckling of Grid Stiffened Composite Shells based on First-order Shear Deformation Theory. *Modares Mech Eng J* 2013; 13(10): 51–61.

[13] Reddy JN. **Mechanics of laminated composite plates and shells: theory and analysis**, CRC Press; 2004.

[14] Qatu MS, **Vibration of laminated shells and plates**: Academic Press; 2004.